Bull. Mater. Sci., Vol. 40, No. 6, October 2017, pp. 1273–1283
DOI 10.1007/s12034-017-1473-2

Influence of electrodeposition parameters on the characteristics of Mn–Co coatings on Crofer 22 APU ferritic stainless steel

HADI EBRAHIMIFAR* and MORTEZA ZANDRAHIMI
Department of Metallurgy and Materials Science, Faculty of Engineering, Shahid Bahonar University of Kerman, Kerman 76169133, Iran
*Author for correspondence (H.Ebrahimifar@eng.uk.ac.ir)

MS received 21 March 2015; accepted 11 June 2017; published online 16 September 2017

Abstract. Manganese–cobalt coatings are promising candidates for solid oxide fuel cell (SOFC) interconnection applications because of their high conductivity and good oxidation resistance. In the present study, manganese and cobalt are electrodeposited on Crofer 22 APU ferritic stainless steel. The effects of current density, pH, sodium gluconate ($NaC_6H_{11}O_7$) concentration, cobalt sulphate concentration ($CoSO_4{\cdot}7H_2O$) and deposition duration on the microstructure and cathodic efficiency are characterized by means of scanning electron microscopy, weight gain measurements and energy-dispersive X-ray spectrometry, respectively. Results show that increases in current density and deposition duration lead to decrease in current efficiency and deposition rate. Increasing the pH to 2.5 causes an initial rise of current efficiency and deposition rate, followed by subsequent decline. In addition, the increases in sodium gluconate and cobalt sulphate concentrations in the electrolyte solution result in an increase in current efficiency and deposition rate. Moreover, the results demonstrate that the variations in the current density, pH, sodium gluconate ($NaC_6H_{11}O_7$) concentration, cobalt sulphate concentration ($CoSO_4{\cdot}7H_2O$) and duration have a significant effect on grain size, uniformity and the adherence of the coating.

Keywords. Electrodeposition; manganese; cobalt; coating; current efficiency.

1. Introduction

Solid oxide fuel cells (SOFCs) are an attractive choice for power generation due to their fuel flexibility and excellent system efficiencies. Recent developments in electrolyte materials have reduced the operating temperatures for SOFCs to between 650 and 800°C [1]. At lower operating temperatures, it is practical to employ metals as interconnections due to excellent electrical, thermal conductivity and ease of fabrication [2,3].

Ferritic stainless steels are the most promising candidates for interconnections which are used in SOFCs at 800°C or lower, because of their close CTE match with other components of SOFCs, and cost-effectiveness as compared with other candidates [4–6]. Crofer 22 APU, E-brite, SUS430 and other alloys have been extensively studied in recent years.

However, the excessive growth of chromia and chromium evaporation can lead to cathode poisoning and can shorten the required service life of the SOFC stack.

To solve the afore-mentioned problems, protective and conductive coatings can be employed. Spinels containing cobalt and manganese, such as $(Mn,Co)_3O_4$ [7–13], $(Cu,Mn)_3O_4$ [12,13] and Co_3O_4 [14], are the best candidates for coating interconnections. Numerous techniques have been developed to apply such coatings to ferritic stainless steel, including slurry coatings [7–10], anodic electrodeposition [11], cathodic electrodeposition [12–14] and pack cementation [15–17]. Several attempts have been made in the electrodeposition of Mn–Co onto ferritic stainless steel for SOFC interconnection applications [12,18–20]. However, so far, no research has been conducted to investigate the effects of electrolysis factors on the deposition of Mn–Co alloys onto Crofer 22 APU.

In this research, the effects of the current density, pH, sodium gluconate concentration, cobalt sulphate concentration and duration on the electrodeposition of Mn–Co alloys onto Crofer 22 APU were investigated.

2. Experimental

2.1 *Substrate preparation*

Coupons of Crofer 22 APU were used as the substrate, whose chemical composition is listed in table 1. Small square-shaped substrate pieces with the dimensions $10 \times 10 \times 2$ mm^3 were wire-cut from 2-mm-thick steel plates. Prior to the deposition, the specimens were polished using a 320- up to a 2,400-grit sic paper, ultrasonically cleaned in ethanol for 10 min and dried. The steel substrates were electropolished at a current density of 500 mA cm^{-2} for 2 min in a H_3PO_4 solution (Merk, 85 vol%). Then, the samples were pickled in a mixed 5% nitric acid (Merk, 65 vol%) and 25% hydrochloric acid (Merk, 37 vol%) solution for 1 min just before use.

2.2 *Electrodeposition of manganese–cobalt*

A one-compartment cell was used for the direct current (DC) electrodeposition process. A platinum foil was used as the anode and was placed in the same compartment of the working electrode. During the deposition, the solution remained unchanged and no inert gas was used to purge the electrolyte. All the experiments were carried out in 100 ml of electrolytes prepared with deionized water. The pH of the electrolytes was adjusted using either ammonia hydroxide (Merk, 29 vol%) or 20 vol% H_2SO_4 (Merk, 98%).

The constant compositions and constant operating conditions for the Mn–Co electrodeposition in all the tests are given in table 2 [18]. Electrodeposition factors, including the current density (table 3), pH (table 4), sodium gluconate (Merk, >99%) concentration (table 5), cobalt(II) sulphate heptahydrate (Merk, >99%) concentration (table 6) and duration (table 7) of the electrodeposition, were investigated for the synthesis of the coatings, which are summarized in tables 3–7. After the electrodeposition, the working electrodes were rinsed with deionized water and dried in air.

Table 1. Chemical composition of Crofer 22 APU ferritic stainless steel.

Element	Concentration (wt%)
Fe	Bal.
C	0.01
Cr	22.7
Mn	0.38
Si	0.02
Ni	0.02
Al	0.02
Ti	0.07
La	0.06

2.3 *Characterization*

The surface morphology, microstructure and chemical composition of the coated specimens were analysed using scanning electron microscopy (SEM) (Camscan MV2300) with energy-dispersive spectroscopy (EDS).

3. Results and discussion

3.1 *Effect of current density*

Bath electroplating with the composition of 0.5 M $MnSO_4$ (111.53 g l^{-1}) + 0.1 M $CoSO_4$ (28.11 g l^{-1}) + 1 M H_3BO_3 (61.84 g l^{-1}) + 0.7 M $NaC_6H_{11}O_7$ (152.7 g l^{-1}) + 0.1 M $(NH_4)_2SO_4$ (13.2 g l^{-1}) was used for the electrodeposition of Mn–Co coating. Manganese sulphate and cobalt sulphate were used, respectively, as sources for Mn^{2+} and Co^{2+} ions. Sodium gluconate was used as a chelating agent, and boric acid was added as a buffer to control the pH at the cathode–solution interface [21].

The addition of ammonium sulphate to electrolyte for manganese electrodeposition is necessary to produce manganese coatings with good coverage. Ammonium sulphate inhibits the precipitation of manganese hydroxide, improves conductivity of the electrolyte and increases the current efficiency [22,23].

Currents of different densities were applied to investigate the morphology and quality of Mn–Co coatings. Figure 1

Table 2. Constant chemical compositions and constant operating conditions for Mn–Co electrodeposition in all tests.

Manganese sulphate trihydrate ($MnSO_4 \cdot 3H_2O$) (Merk, >98%)	111.53 g l^{-1} (0.5 M)
Boric acid (H_3BO_3) (Merk, >99%)	61.84 g l^{-1} (1 M)
Ammonium sulphate $(NH_4)_2SO_4$ (Merk, >99%)	13.2 g l^{-1} (0.1 M)
Temperature	25°C
Agitation	Magnetic bar from the bottom
Anode	Platinum foil

Table 3. Investigating the effect of current density on the electrodeposition of Mn–Co coating.

Number	i (mA cm^{-2})	pH	Duration (min)	$NaC_6H_{11}O_7$ (M)	$CoSO_4 \cdot 7H_2O$ (M)
1	150	2.5	20	0.7	0.1
2	200	2.5	20	0.7	0.1
3	250	2.5	20	0.7	0.1
4	300	2.5	20	0.7	0.1

Table 4. Investigating the effect of pH on the electrodeposition of Mn–Co coating.

Number	i (mA cm^{-2})	pH	$NaC_6H_{11}O_7$ (M)	$CoSO_4{\cdot}7H_2O$ (M)
1	250	2	0.7	0.1
2	250	2.5	0.7	0.1
3	250	2.75	0.7	0.1
4	250	3	0.7	0.1
5	250	3.5	0.7	0.1

Table 5. Investigating the effect of sodium gluconate on the electrodeposition of Mn–Co coating.

Number	i (mA cm^{-2})	pH	Duration (min)	$NaC_6H_{11}O_7$ (M)	$CoSO_4{\cdot}7H_2O$ (M)
1	250	2.5	20	0.2	0.1
2	250	2.5	20	0.6	0.1
3	250	2.5	20	0.7	0.1
4	250	2.5	20	1	0.1

Table 6. Investigating the effect of cobalt sulphate on the deposition of Mn–Co coating.

Number	i (mA cm^{-2})	pH	Duration (min)	$NaC_6H_{11}O_7$	$CoSO_4{\cdot}7H_2O$ (M)
1	250	2.5	20	0.7	0.01
2	250	2.5	20	0.7	0.05
3	250	2.5	20	0.7	0.1
4	250	2.5	20	0.7	0.2

Table 7. Investigating the effect of duration on the deposition of Mn–Co coating.

Number	i (mA cm^{-2})	pH	Duration (min)	$NaC_6H_{11}O_7$ (M)	$CoSO_4{\cdot}7H_2O$ (M)
1	250	2.5	10	0.7	0.1
2	250	2.5	20	0.7	0.1
3	250	2.5	30	0.7	0.1

shows the surface morphology of the coating, which was deposited under different current densities (table 3; i = 100, 150, 200, 250 and 300 mA cm^{-2}). It is obvious that on increasing the current density, the grain size is decreased. Figure 1a demonstrates the substrate electroplated at a current density of 100 mA cm^{-2}. As can be seen, the coating is non-uniform, and some cracks are observed. The coating obtained at i = 150 mA cm^{-2} is more uniform than the coating obtained at the current density of 100 mA cm^{-2}. On increasing the current density further, the coating becomes more uniform, and the grain size is decreased. At i = 300 mA cm^{-2}, the coating is non-uniform and some parts of the specimen are not coated.

The surface roughness coating obtained by electrodeposition is changed with an over-potential [24–26]. Indeed, the surface roughness is high at low over-potentials and becomes lower at high over-potentials. Low over-potential (low current density) depositions produce coatings with large surface irregularities, whereas high over-potential depositions produce coatings with smooth surfaces [27].

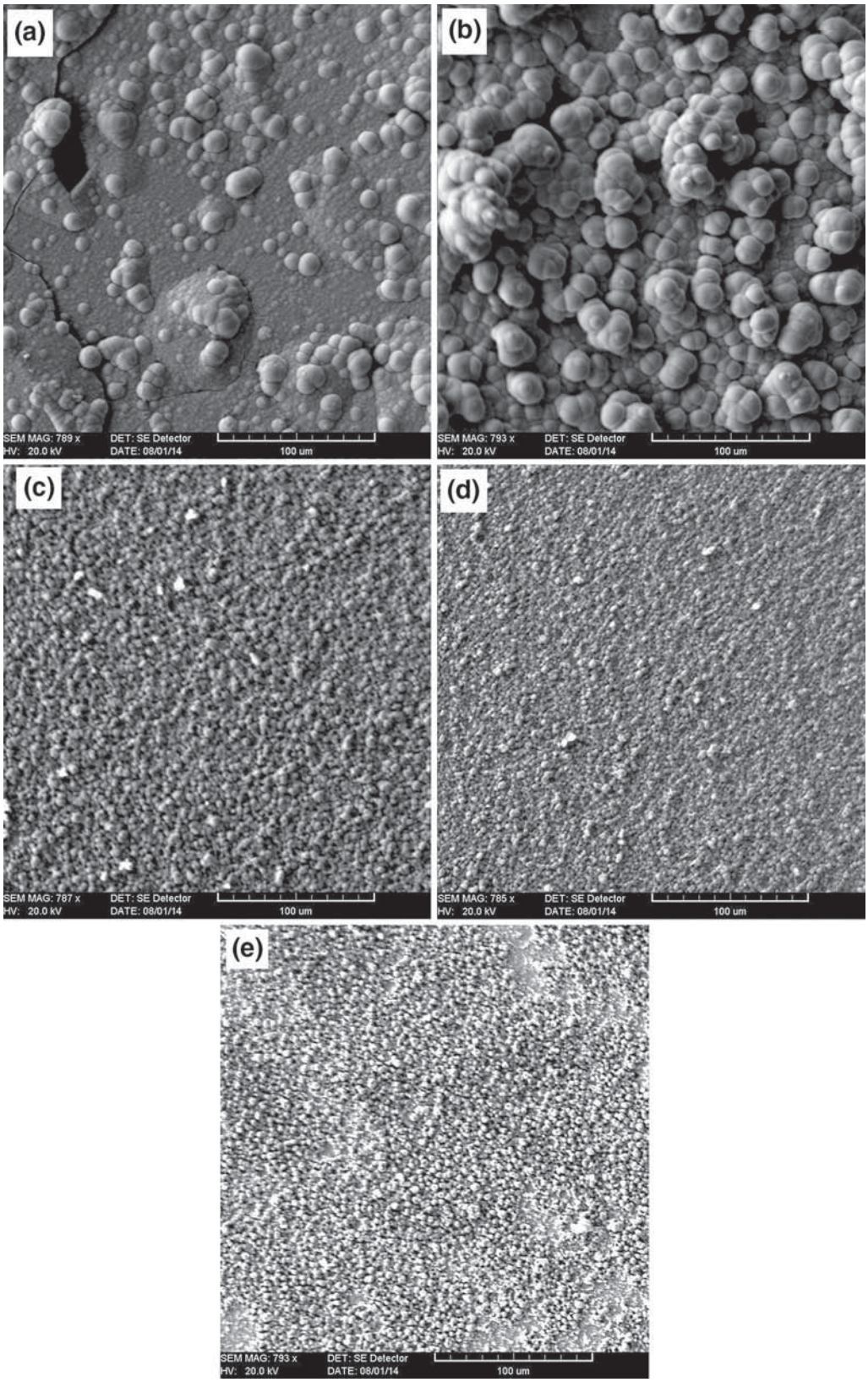

Figure 1. SEM surface morphology of coatings after 20 min electrodeposition at different current densities in solution of 0.5 M $MnSO_4$ + 0.1 M $CoSO_4$ + 1 M H_3BO_3 + 0.7 M $NaC_6H_{11}O_7$ + 0.1 M $(NH_4)_2SO_4$ at pH 2.5: (**a**) 100, (**b**) 150, (**c**) 200, (**d**) 250 and (**e**) 300 mA cm^{-2}.

Furthermore, the surface roughness changes with current density. The number of metal ion discharge events per unit area or per unit time is small at low current densities. Even at low current densities, the metal ion discharge event will still occur preferentially at protrusions [27]. These protrusions will grow, producing coatings with high surface irregularities. At high current densities, high densities of metal ions (Mn^{2+} and Co^{2+}) are discharged on the cathode surface.

At high current densities, if charged particles are brought closer than the critical distance, they repel. The high densities of the metal ions and electrons generated at high current densities will be redistributed over the surface according to the magnitude of their repulsive force. This cation redistribution over the substrate surface allows the discharge sites to be more uniformly distributed, smoothening the surface of the coating [27].

The results of EDX analysis showed that the amount of oxygen is negligible for the coating obtained at current density $i = 100, 150, 200$ and 250 mA cm^{-2}. The amount of oxygen for the coating obtained at the current density of 250 mA cm^{-2} was 10.26%, indicating the formation of oxide/hydroxides.

The formation of hydroxide indicates that pH values have reached a range that the buffer cannot control. However, although finding $Co(OH)_2$ was expected, only $Mn(OH)_2$ was present in the coatings. There are two possible reasons for this. Firstly, the low concentration of cobalt in the solution indicates that cobalt has already reached its diffusion control limit, which makes the concentration of cobalt at the surface where pH is the highest very low near the cathode surface. Therefore, much higher pH value is required to form $Co(OH)_2$. The other possibility is that $Co(OH)_2$ may be reduced to cobalt directly by reaction (1) at –0.73 V *vs.* SHE. Although Mn could also be produced by reducing $Mn(OH)_2$, the deposition potential is –1.55 V *vs.* SHE, which is more negative than that of $Co(OH)_2$ and even more negative than that of Mn^{2+} reduction (−1.18V *vs.* SHE) [28–32].

$$Co^{2+} + 2OH^- = Co(OH)_2 + 2e^- \ (E_o = -0.73\ V_{SHE}) \quad (1)$$

$$Mn^{2+} + 2OH^- = Mn(OH)_2 + 2e^- \ (E_o = -1.55\ V_{SHE}) \quad (2)$$

For measuring the current efficiency, equation (3) was used [33]:

$$CE = \frac{m_e}{m_t}, \quad (3)$$

where m_e is the measured weight of the deposit and m_t is the theoretical weight of deposit, which is calculated as follows:

$$m_t = \frac{MIt}{nF}, \quad (4)$$

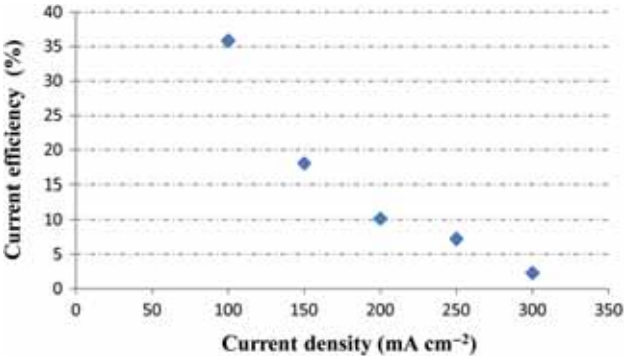

Figure 2. Effect of current density on current efficiency at pH 2.5 for bath containing 0.5 M $MnSO_4$ + 0.1 M $CoSO_4$ + 1 M H_3BO_3 + 0.7 M $NaC_6H_{11}O_7$ + 0.1 M $(NH_4)_2SO_4$.

where M is the atomic mass, I is the current density, t is the time, n is the number of exchanged equivalents and F is Faraday's constant.

Figure 2 shows the effect of the current density on the cathode efficiency. On increasing the current density, the cathode efficiency is decreased. For the deposition of the Mn–Co coating, four reactions could occur [18]:

$$2H^+ + 2e^- \rightarrow H_2 \quad (5)$$

$$Co^{2+} + 2e^- \rightarrow Co \ (E_o = -0.277\ V_{SHE}) \quad (6)$$

$$2H_2O + 2e^- \rightarrow H_2 + 2OH^- \ (E_o = -0.827\ V_{SHE}) \quad (7)$$

$$Mn^{2+} + 2e^- \rightarrow Mn \ (E_o = -1.118\ V_{SHE}) \quad (8)$$

Reactions (5) and (7) result in a lack of deposition and waste current; at high current densities, more hydrogen bubbles are produced, resulting in a lower current efficiency and a lower deposition rate, consistent with the changes of surface morphology with current densities.

3.2 *Effect of pH*

The effect of the electrolyte pH on the surface morphologies of the Mn–Co coatings was investigated using SEM. SEM micrographs of these coatings electroplated at different pH levels (table 4; pH = 2, 2.5, 2.75, 3 and 3.5) are shown in figure 3. At pH = 2, the coating is discontinuous and non-uniform (figure 3a), while the coating obtained at pH = 2.5 is uniform and continuous (figure 1d). The surface morphology of the coating obtained at pH = 2.75 (figure 3b) is uniform and continuous compared with the coating produced at pH = 2. However, some parts of the substrate are uncoated, which is obvious at higher magnifications (figure 3c). With further increases in the pH to 3 (figure 3d) and 3.5 (figure 3e), the discontinuity is increased. Figure 4 shows the current efficiency *vs.* pH. The current efficiency increases on increasing the pH from 2 to 2.5 and it then decreases, which is consistent with the surface morphologies (figure 3).

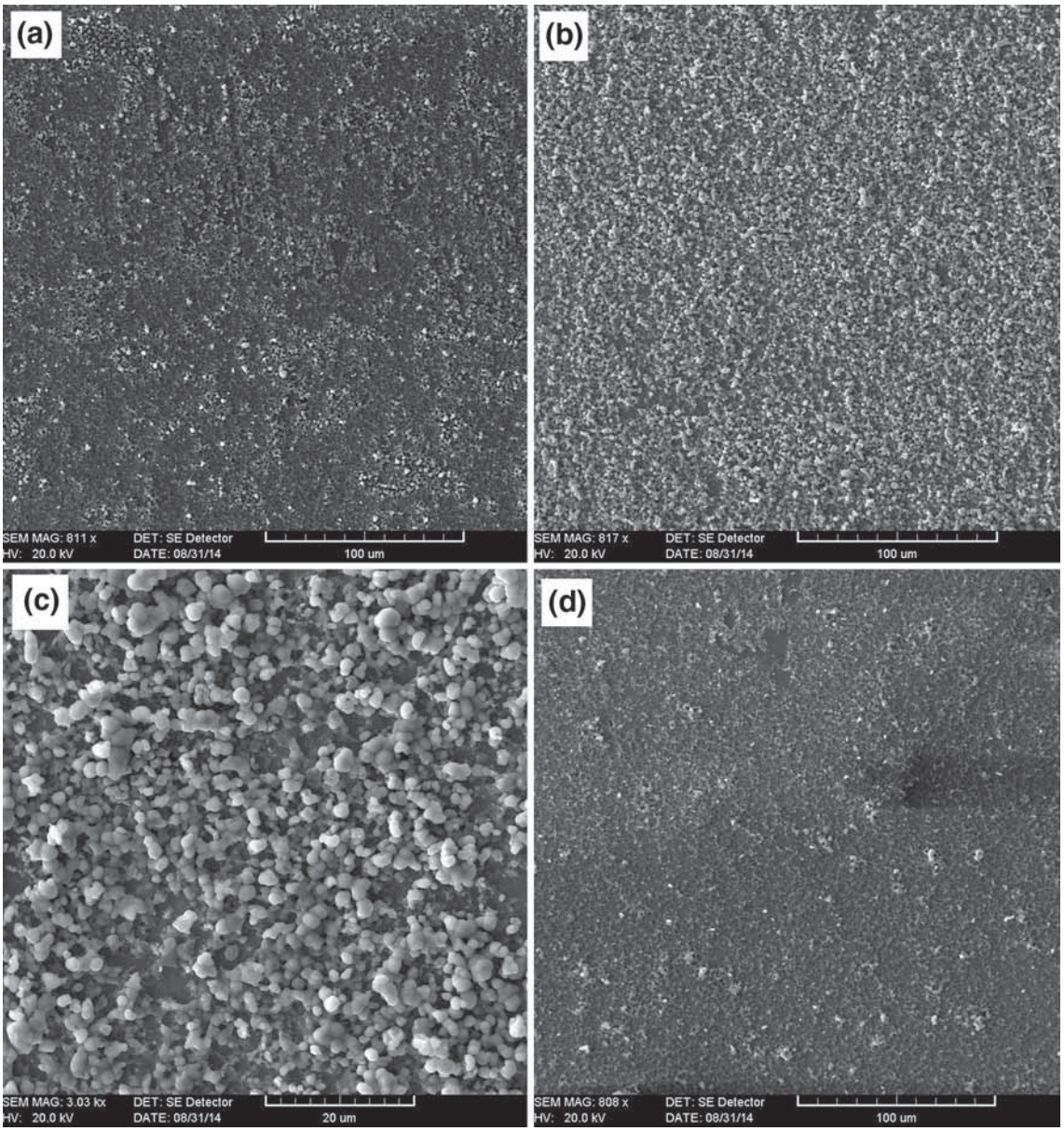

Figure 3. SEM surface morphology of coatings after 20 min electrodeposition at different pH in solution of 0.5 M $MnSO_4$ + 0.1 M $CoSO_4$ + 1 M H_3BO_3 + 0.7 M $NaC_6H_{11}O_7$ + 0.1 M $(NH_4)_2SO_4$ at current density of 250 mA cm^{-2}: (**a**) pH = 2, (**b**) pH = 2.75, (**c**) higher magnification of part b, (**d**) pH = 3 and (**e**) pH = 3.5.

The results of EDX revealed that the amount of oxygen in the coatings obtained from pH = 3 and pH = 3.5 is high (5.93 and 14.34, respectively). The presence of oxygen probably indicates the formation of oxide/hydroxides in the coatings. In aqueous electrolytes, manganese reacts with water, resulting in hydrogen evolution and formation of surface manganese oxide or hydroxide (MnO or $Mn(OH)_2$) [34]:

$$Mn + H_2O \rightarrow MnO + H_2 \quad (9)$$

or

$$Mn + 2H_2O \rightarrow Mn(OH)_2 + H_2 \quad (10)$$

In the presence of H^+ or NH_4^+, the formation of surface oxide can be suppressed according to the following reactions:

$$MnO + 2H_3O^+ \rightarrow Mn^{2+} + 3H_2O \quad (11)$$

$$MnO + 2NH_4^+ \rightarrow Mn(NH_3)^{2+} + H_2O \quad (12)$$

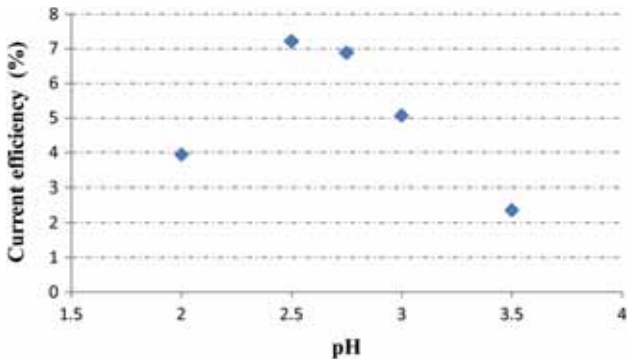

Figure 4. Effect of pH on current efficiency at current density of 250 mA cm^{-2} for bath containing 0.5 M $MnSO_4$ + 0.1 M $CoSO_4$ + 1 M H_3BO_3 + 0.7 M $NaC_6H_{11}O_7$ + 0.1 M $(NH_4)_2SO_4$.

The formation of oxide/hydroxide layers leads to an increase in the over-potential of Mn (II) discharge. The overall kinetics of the deposition reaction is determined by the balance between rates of manganese oxidation and activation reactions. Since the removal of the oxide/hydroxide layer is probably the slowest and is a potential-independent reaction, an unfavourable balance between inhibition and activation reactions at sufficiently negative potentials may result in kinetic limitation of the overall rate of deposition reaction. An additional factor affecting the inhibition/activation balance may be due to electrochemical reaction of hydrogen evolution. At a low over-potential, water is discharged while at a high over-potential, the discharge of ammonium ion becomes more favourable. This is in agreement with the findings reported by Suliakas *et al* [35].

For aqueous electrolytes containing $MnSO_4$ and $(NH_4)_2SO_4$, Mn^{2+} can exist in unstable complex forms $[Mn(H_2O)_6]^{2+}$, $[Mn(NH_3)_{x=1-6}]^{2+}$ and $[Mn(H_2O)_{6-n}(NH_3)_n]^{2+}$. It is also proposed that Mn^{2+} discharge could take place through the following mechanism (reactions (9) and (10)) in the presence of NH_3 [36–41]:

$$[Mn(H_2O)_{6-n}(NH_3)_n]^{2+} + xH_2O \rightarrow [Mn(H_2O)_{6-n+x}]^{2+} + nNH_3 \quad (13)$$

$$[Mn(H_2O)_{6-n+x}]^{2+} + 2e^- \rightarrow Mn + (_{6-n+x})H_2O \quad (14)$$

Therefore, the addition of ammonium sulphate leads to the formation of appropriate complex forms of Co^{2+} and Mn^{2+} as well as improvement of Mn and Co co-deposition. Deans studies showed that as pH increases during electrodeposition, ammonium sulphate inhibits the precipitation of Mn hydroxides [42].

It is expected that at a lower pH, Mn^{2+} exists mainly as $[Mn(H_2O)_6]^{2+}$, and at a higher pH, it is $[Mn(H_2O)_{6-n}(NH_3)_n]^{2+}$ [35–40]. Therefore, at a low pH, the formation of proper complexes for the co-deposition of Mn and Co leads to an increase in the current efficiency rate. It should be considered that at a low pH, Mn ions are only in a hydrated form. In addition, it is well known that the ammonium sulphate concentration is affected by the electrolyte pH [39]. Therefore, a pH above 2.5 and the presence of Mn hydroxide $[Mn(OH)_2]$ and Co hydroxide $[Co(OH)_2]$ and their oxidation products make the solution unclear and decrease the current efficiency, which is harmful for the co-deposition of Mn–Co. Another reason for the increased current efficiency due to the increase in the pH and the decreased current efficiency due to the increase in the pH is the concentration of H^+ in the electrolyte. With the increase in pH, the release of hydrogen is decreased; therefore, the current efficiency and deposition rate are increased. At a higher pH, the formations of manganese/cobalt hydroxides and their products cause lower metallic cations (Mn^{2+} and Co^{2+}) and an unclear solution. The formation of such compositions decreases the current efficiency and deposition rate, which is consistent with the present experimental tests.

3.3 *Effect of sodium gluconate*

To clarify on what chelating level is required for the co-deposition of Mn–Co, different amounts of chelating agents (sodium gluconate) were used. The surface morphologies of the coated samples for different amounts of sodium gluconate (0.2, 0.4, 0.7 and 1 M sodium gluconate) are shown in figure 5. At 0.2 M of sodium gluconate, the coating is non-continuous and some parts of the substrate are uncoated (figure 5a). The coating obtained in the 0.4 M sodium gluconate solution (figure 5b) is more continuous and uniform than the coating obtained in the 0.2 M solution. At higher magnifications, some pores are observed in the surface of the coating obtained in the 0.4 M sodium gluconate solution (figure 5c). Neither a discontinuity nor cracks are observed in the coating achieved from 0.7 M (figure 1d) and 1 M sodium gluconate solutions (figure 5d). The grain size of the coating obtained from the 1 M sodium gluconate solution is larger than the coating achieved from the 0.7 M solution. Table 8 demonstrates the EDX results obtained for the deposited surface after the deposition. The presence of Fe and Cr is related to the substrate because of the thin coating or discontinuities in the coating. The presence of oxygen probably indicates the formation of Mn/Co hydroxides. At a low amount of sodium gluconate (0.2 and 0.4 M), the amount of manganese is low because of fewer chelating agents to chelate with manganese [18].

A chelating agent was used to stabilize cobalt and manganese and to prevent the formation of hydroxides [32,43,44]. During the preparation of solution electrolyte, cobalt was chelated with gluconate first, before manganese sulphate was added. According to reference [45], Co^{2+} is present mainly as $[Co(C_6H_{11}O_7)]^+$ complex; gluconate ion is attached to Co^{2+} by coordination through the carboxyl group and one of the adjacent hydroxyl groups. Addition of gluconate reduces the free cation concentrations; therefore, the pH value for hydroxide formation is increased.

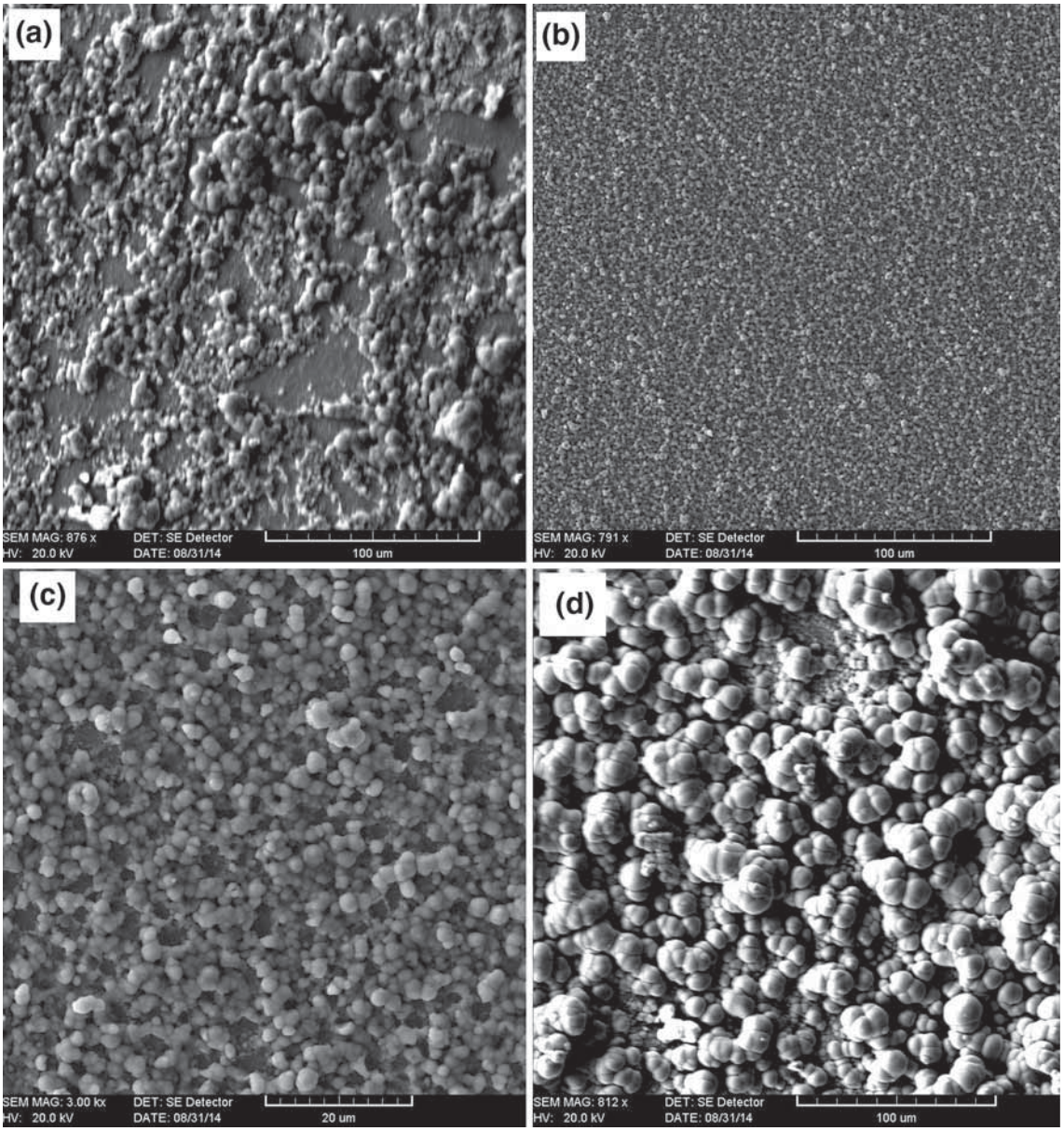

Figure 5. SEM surface morphology of coatings after 20 min electrodeposition with different sodium gluconate contents in solution of 0.5 M $MnSO_4$ + 0.1M $CoSO_4$ + 1 M H_3BO_3 + 0.1 M $(NH_4)_2SO_4$ at pH 2.5 and current density of 250 mA cm^{-2}: (**a**) 0.2 M $NaC_6H_{11}O_7$, (**b**) 0.4 M $NaC_6H_{11}O_7$, (**c**) higher magnification of part c and (**d**) 1M $NaC_6H_{11}O_7$.

Table 8. Chemical composition of coatings obtained in electrolyte solution with different amounts of gluconate.

Gluconate (M)	Co (wt%)	Mn (wt%)	O (wt%)	Fe (wt%)	Cr (wt%)
0.2	38.26	7.52	17.05	28.91	8.26
0.4	44.14	15.95	14.22	19.45	6.24
0.7	50.84	43.64	0.74	3.46	1.32
1	54.32	44.83	0.85	0	0

After all the cobalt was chelated, the remainder of the gluconate was able to chelate with Mn^{2+} [18]. If all the manganese and cobalt cations are chelated, no hydroxide can precipitate on the substrate surface during deposition, even if the pH goes outside the range of pH buffer. Therefore, the low amount of manganese (table 8) was due to the low amount of gluconate. However, considering the lower chelating effect of gluconate with manganese, it is important to add enough amount of gluconate to make sure that the chelation is complete. This is consistent with the data in table 8; only solutions with enough amounts of gluconate (0.7 and 1 M) avoid hydroxide formation.

Furthermore, the effect of boric acid should be considered. Boric acid plays a greater role than merely as a buffer. It is believed that boric acid complexes with Co^{2+} ions acting as a homogeneous catalyst or adsorbs on the electrode surface [46–48] which lowers the over-potential for cobalt deposition. Scharifker and Hills [49] suggested that boric acid is adsorbed on the cathode surface, and thus decreases the active area for hydrogen evolution, thus affecting the resulting morphology characteristics of the deposits. Hence, the co-existence of gluconate and boric acid improves the co-deposition of Mn–Co alloy.

To achieve a uniform and continuous coating with lower amounts of hydroxide or oxide, a sufficient amount of gluconate is needed. The amount of oxygen in the coating obtained from 0.7 M of gluconate in the solution is significantly increased, indicating trace amounts of hydroxides. At higher amounts of sodium gluconate (1 M and higher), the amounts of cobalt, manganese and oxygen are not very different from 0.7 M of gluconate. Therefore, 0.7 M of gluconate in the electrolyte solution is sufficient for obtaining approximately equal amounts of manganese and cobalt in the coating composition. In addition, the grain size with 1 M of gluconate is larger than that with 0.7 M. One cause of the growth of such coarse grains could be a higher deposition rate. Such relatively coarse grains obtained from 1 M of the sodium gluconate solution is harmful during SOFC operation. The coarse grains cause a lower oxidation resistance [50–52]. With the decrease in grain size, the adherence of the coating to the substrate is improved, which will result in a better oxidation resistance. Figure 6 illustrates the current efficiency as a function of sodium gluconate amount. On increasing the amount of sodium gluconate, the current efficiency is increased. At a higher amount of sodium gluconate, the deposition rate is increased, which results in a thicker coating. Therefore, the experimental weight gain of the deposition is enhanced, which is consistent with the SEM micrographs (figure 5).

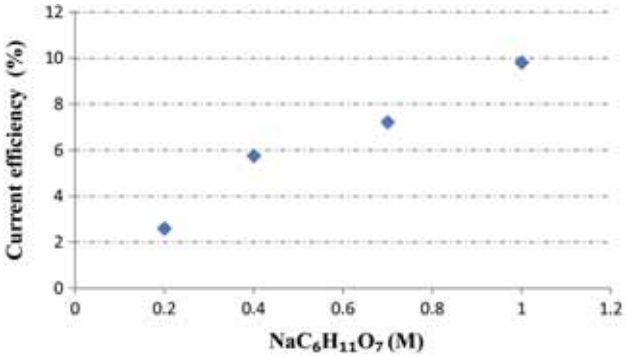

Figure 6. Effect of sodium gluconate on current efficiency at pH 2.5 and current density of 250 mA cm^{-2} for bath containing 0.5 M $MnSO_4$ + 0.1 M $CoSO_4$ + 1 M H_3BO_3 + 0.1 M $(NH_4)_2SO_4$.

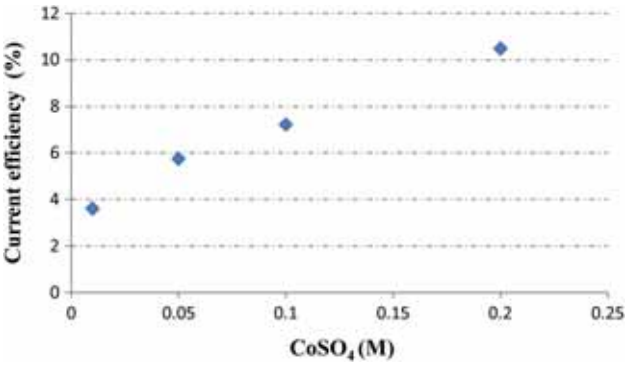

Figure 7. Effect of cobalt sulphate on current efficiency at pH 2.5 and current density of 250 mA cm^{-2} for bath containing 0.5 M $MnSO_4$ + 0.1 M $CoSO_4$ + 1 M H_3BO_3 + 0.7 M $NaC_6H_{11}O_7$ + 0.1 M $(NH_4)_2SO_4$.

3.4 *Effect of cobalt sulphate*

To investigate the effect of cobalt sulphate on the coating, different amounts of $CoSO_4$ (0.01, 0.05, 0.1 and 0.2 M $CoSO_4$) in the electrolyte were studied (table 6). The coating obtained in 0.01 and 0.05 M of cobalt sulphate solution was non-uniform and discontinuous. In addition, some parts of the substrate were bare because of the low amount of cobalt sulphate in the solution. With the increase of sulphate cobalt to 0.1 M, the coating grew uniformly and became continuous (figure 1d). At a higher amount of cobalt sulphate (0.2 M), the deposition rate was so high that a coarse layer was produced. Similarly, the grain size was larger than that in the coatings obtained with lower amounts of cobalt sulphate in the solution. In addition, the high deposition rate produced some stresses in the coating, which led to cracking [53]. Moreover, based on the EDX observations, the amount of cobalt in the coating is high and the manganese content is low. For the formation of Mn–Co spinels during oxidation, a higher amount of manganese is needed. In addition, such a coarse coating with large grains will result in a lower oxidation resistance than a coating with smaller grains [50–52]. The current efficiency as a function of $CoSO_4$ is shown in figure 7. On increasing the cobalt sulphate, the current efficiency is enhanced, the deposition rate increases and, for constant duration of 20 min, it results in a thicker coating. Therefore, the experimental weight gain of the coating increases and causes higher current efficiencies.

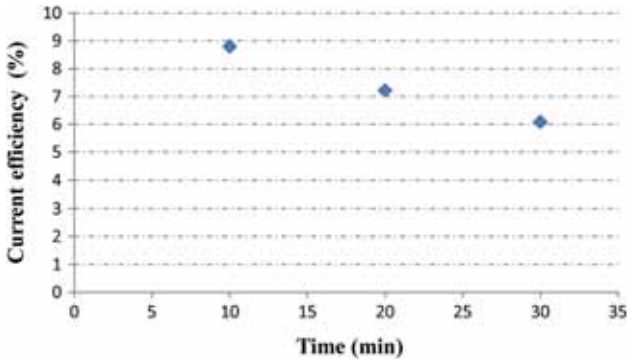

Figure 8. Effect of electrodeposition duration on current efficiency at pH 2.5 and current density of 250 mA cm^{-2} for bath containing 0.5 M $MnSO_4$ + 0.1 M $CoSO_4$ + 1 M H_3BO_3 + 0.7 M $NaC_6H_{11}O_7$ + 0.1 M $(NH_4)_2SO_4$.

3.5 *Effect of duration*

In order to investigate the effect of deposition time, deposition was conducted for different durations (10, 20 and 30 min) was studied. The deposited layer after 10 min was non-uniform and continuous. After 20 min of electrodeposition, the coating was uniform with no cracks (figure 1d). The coating obtained after 30 min of electrodeposition was relatively uniform; however, some cracks were observed in the surface of the coating. Moreover, after 30 min of electroplating, the solution was dark and unclear. At lower durations, the deposition duration is insufficient to coat all parts of the substrate; therefore, some areas remains bare. At higher durations, the coating thickens and the residual stresses in the coating cause the coating to crack [53]. In addition, on increasing the duration for a particular solution, unwanted reactions occur (perhaps the formation of hydroxides or oxides), which result in a dark and unclear solution. The current efficiency as a function of the deposition duration is demonstrated in figure 8. On increasing the deposition duration, the current efficiency is decreased, which could be related to Faraday's law [33]. At higher durations, the weight gain of the deposition should be higher in relation with the theoretical weight gain based on Faraday's law. Therefore, in a constant solution based on equation (3), due to the increase in the deposition duration, current efficiency is decreased. Furthermore, for a particular solution, over time, the concentration of Co^{2+}/Mn^{2+} in the solution decreases, resulting in a lower current efficiency. The reduction in cations in the solution also reduces the deposition rate.

Based on the SEM micrographs and EDX results, the coating obtained in the solution of 0.50 M $MnSO_4$ + 0.10 M $CoSO_4$ + 1.0 M H_3BO_3 + 0.70 M gluconate + 0.10 M $(NH_4)_2SO_4$ is optimum. Also, the best current density, pH and deposition duration obtained are found to be 250 mA cm^{-2}, 2.5 and 20 min, respectively.

4. Conclusions

Crofer 22 APU ferritic stainless steel was electrodeposited with manganese and cobalt simultaneously. The effects of current density, pH, sodium gluconate, cobalt sulphate and duration of deposition on the morphology of deposited coatings were investigated. Results demonstrated that these parameters have significant influence on the microstructure of deposited coatings. Increase of current density, sodium gluconate and cobalt sulphate and duration of electrodeposition resulted in uniform and homogeneous deposit. At high pH (3, 3.5), the coating was not uniform. The optimum current density, pH and deposition duration were 250 mA cm^{-2}, 2.5 and 20 min, respectively. Also for obtaining uniform coating whithout cracking, the concentration of sodium gluconate and cobalt sulphate should be 0.7 and 0.1 M, respectively.

References

[1] Magdefrau N J, Chen L, Sun E Y and Aindow M 2013 *J. Power Sources* **241** 756
[2] Fergus J W 2005 *Mater. Sci. Eng. A* **397** 271
[3] Zhang H, Wu J, Liu X and Baker A 2013 *Int. J. Hydrog. Energy* **38** 5075
[4] Wu J, Gemmen R S, Manivannan A and Liu X 2011 *Int. J. Hydrog. Energy* **36** 4525
[5] Yang Z, Weil K S, Paxton D M and Stevenson J W 2003 *J. Electrochem. Soc.* **150** A1188
[6] Ebrahimifar H and Zandrahimi M 2012 *Ionics* **18** 615
[7] Chen X, Hou, P Y, Jacobson C P, Visko S J and De Jonghe L C 2005 *Solid State Ion.* **176** 425
[8] Yang Z, Xia G, Simner S P and Stevenson J W 2005 *J. Electrochem. Soc.* **152** 1896
[9] Yang Z, Xia G, Li X and Stevenson J W 2007 *Int. J. Hydrog. Energy* **32** 3648
[10] Yang Z, Xia G and Stevenson J W 2005 *Electrochem. Solid-State Lett.* **8** A168
[11] Wei W, Chen W and Ivey D G 2007 *Chem. Mater.* **19** 2816
[12] Bateni M R, Wei P, Deng X and Petric A 2007 *Surf. Coat. Technol.* **201** 4677
[13] Wei P, Deng X, Bateni M R and Petric A 2007 *Corrosion* **63** 529
[14] Deng X, Wei P, Bateni M R and Petric A 2006 *J. Power Sources* **160** 1225
[15] Zandrahimi M, Vatandoost J and Ebrahimifar H 2012 *J. Mater. Eng. Perform.* **21** 2074
[16] Ebrahimifar H and Zandrahimi M 2011 *Indian J. Eng. Mater. Sci.* **18** 314
[17] Zandrahimi M, Vatandoost J and Ebrahimifar H 2011 *Oxid. Met.* **76** 347
[18] Wu J, Jiang Y, Johnson C and Liu X 2008 *J. Power Sources* **177** 376
[19] Fu Q X, Sebold D, Tietz F and Buchkremer H P 2011 *Solid State Ion.* **192** 376
[20] Wu J, Johnson C D, Gemmen R S and Liua X 2009 *J. Power Sources* **189** 1106

[21] Karwas C and Hepel T 1989 *J. Electrochem. Soc.* **136** 1672
[22] Gong J and Zangari G 2002 *J. Electrochem. Soc.* **149** C209
[23] Dean R S 1952 *Electrolytic manganese and its alloys* (New York: Ronald Press Company)
[24] Inoue K, Nakata T and Watanabe T 2002 *Mater. Trans. Jap. Inst. Met.* **43** 1318
[25] Ohno I and Haruyama S 1991 *J. Jpn. Inst. Met.* **30** 735
[26] Winand R 1994 *Electrochim. Acta* **38** 1091
[27] Watanabe T 2004 *Nano-plating: microstructure control theory of plated film and data base of plated film microstructure,* 1st ed (Amsterdam: Elsevier)
[28] Gong J and Zangari G 2003 *Mater. Sci. Eng. A* **344** 268
[29] Brenner A 1963 *Electrodeposition of alloys* vol. II (New York: Academic Press)
[30] Chen K and Wilcox G D 2006 *J. Electrochem. Soc.* **153** C634
[31] Gong J and Zangari G 2004 *J. Electrochem. Soc.* **151** C297
[32] Cohen-Hyams T, Kaplan W D, Aurbach D, Cohen Y S and Yahalom J 2003 *J. Electrochem. Soc.* **150** 28
[33] Lee C, Lem J, Hwang S, Park E and Shim J 2009 *Trans. Nonferrous Met. Soc. China* **19** 965
[34] Heusler K E and Burgmann M 1970 *Electrochim. Acta* **15** 1887
[35] Suliakas A, Yanitskii J and Viskelis P 1984 *Lietuvos TSR Mokslu Akad. Darbai Serija B: Chem. Tech. Fiz. Geogr.* **5** 25
[36] Boucher L J, Gmelin L, Koeber K and Tille D 1988 *Gmelin handbook of inorganic chemistry* 8th ed (Heidelberg: Springer)
[37] Reedijk J and Poeppelmeier K 2013 *Comprehensive inorganic chemistry II* 2nd ed (Amsterdam: Elsevier Science BV)
[38] Huerta D, Zhouping A, Luo P and Heusler K E 1994 *Electrochim. Acta* **39** 2795
[39] Ananth M V 1997 *Trans. Inst. Met. Finish.* **75** 224
[40] Sriveeraraghavn S, Krishnan R M, Natarajan S R, Parthasaradhy N V and Udupa H V K 1979 *Met. Finish.* **77** 57
[41] Mangolini F, Magagnin L and Cavalloti P L 2006 *J. Electrochem. Soc.* **153** C623
[42] Beatty R 2004 *Manganese elements* (United States: Benchmark Books)
[43] Gong J and Zangari G 2003 *Mater. Sci. Eng. A* **344** 268
[44] Chen K and Wilcox G D 2006 *J. Electrochem. Soc.* **153** C634
[45] Abd El Rehim S S, Ibrahim M A M and Dankeria M M 2002 *J. Appl. Electrochem.* **32** 1019
[46] Abd El Rehim S S, Abd El Wahaab S M, Rashwan S M and Anwar Z M 2000 *J. Chem. Technol. Biotechnol.* **75** 237
[47] Karwas C and Hepel T 1988 *J. Electrochem. Soc.* **135** 839
[48] Horkan J 1979 *J. Electrochem. Soc.* **126** 1861
[49] Scharifker B and Hills G 1983 *Electrochim. Acta* **28** 879
[50] Meng J S and Ji Z S 2014 *Trans. Nonferrous Met. Soc. China* **24** 3571
[51] Cao G J, Xu H Y, Zheng Z Z, Geng L and Masaaki N 2012 *Trans. Nonferrous Met. Soc. China* **22** 1588
[52] Kaplin C and Brochu M 2014 *Appl. Surf. Sci.* **30** 258
[53] Armyanov S and Sotirova G 1982 *Surf. Coat. Technol.* **17** 329